

# Accelerating Fock build via hybrid analytical-numerical integration

Yong Zhang,<sup>†</sup> Rongding Lei,<sup>‡</sup> Bingbing Suo,<sup>\*,‡</sup> and Wenjian Liu<sup>\*,†</sup>

<sup>†</sup>*Qingdao Institute for Theoretical and Computational Sciences, College of Chemistry and  
Chemical Engineering, Shandong University, Qingdao 266237, P. R. China*

<sup>‡</sup>*Shaanxi Key Laboratory for Theoretical Physics Frontiers, Institute of Modern Physics,  
Northwest University, Xi'an 710127, P. R. China*

E-mail: bsuo@nwu.edu.cn; liuwj@sdu.edu.cn

## Abstract

A hybrid analytical-numerical integration scheme is introduced to accelerate the Fock build in self-consistent field (SCF) and time-dependent density functional theory (TDDFT) calculations. To evaluate the Coulomb matrix  $\mathbf{J}[\mathbf{D}]$ , the (induced) density matrix  $\mathbf{D}$  is first decomposed into two parts, the superposition of atomic density matrices  $\mathbf{D}_{\oplus}^A$  and the rest  $\mathbf{D}^R = \mathbf{D} - \mathbf{D}_{\oplus}^A$ . While  $\mathbf{J}[\mathbf{D}_{\oplus}^A]$  is evaluated analytically,  $\mathbf{J}[\mathbf{D}^R]$  is evaluated fully numerically [with the multipole expansion of the Coulomb potential (MECP)] during the SCF iterations. Upon convergence,  $\mathbf{D}^R$  is further split into those of near ( $\mathbf{D}^{RC}$ ) and distant ( $\mathbf{D}^{RL}$ ) atomic orbital (AO) pairs, such that  $\mathbf{J}[\mathbf{D}^{RC}]$  and  $\mathbf{J}[\mathbf{D}^{RL}]$  are evaluated semi-numerically and fully numerically (with MECP). Such a hybrid  $\mathbf{J}$ -build is dubbed ‘analytic-MECP’ (aMECP). Likewise, the analytic evaluation of  $\mathbf{K}[\mathbf{D}_{\oplus}^A]$  and semi-numerical evaluation of  $\mathbf{K}[\mathbf{D}^R]$  are also invoked for the construction of the exchange matrix  $\mathbf{K}[\mathbf{D}]$  during the SCF iterations. The chain-of-spheres (COSX) algorithm [Chem. Phys. 356, 98 (2009)] is employed for  $\mathbf{K}[\mathbf{D}^R]$  but with a revised construction of the S-junctions for overlap AO pairs. To distinguish from the original COSX algorithm (which does not involve the partition of the density matrix  $\mathbf{D}$ ), we denote the presently revised variant as COSx. Upon convergence,  $\mathbf{D}^R$  is further split into those of near ( $\mathbf{D}^{RC}$ ) and distant ( $\mathbf{D}^{RL}$ ) AO pairs followed by a re-scaling, leading to  $\tilde{\mathbf{D}}^{RC}$  and  $\tilde{\mathbf{D}}^{RL}$ , respectively.  $\mathbf{K}[\tilde{\mathbf{D}}^{RC}]$  and  $\mathbf{K}[\tilde{\mathbf{D}}^{RL}]$  are then evaluated analytically and semi-numerically (with COSx), respectively. Such a hybrid  $\mathbf{K}$ -build is dubbed ‘analytic-COSx’ (aCOSx). Extensive numerical experimentations reveal that the combination of aMECP and aCOSx is highly accurate for ground state SCF calculations ( $< 1\mu\text{E}_h/\text{atom}$  error in energy) and is particularly efficient for calculations of large molecules with extended basis sets. As for TDDFT excitation energies, a medium grid for MECP and a coarse grid for COSx are already sufficient.

# 1 Introduction

An efficient Fock build is the prerequisite for electronic structure calculations of large molecular systems.<sup>1</sup> In the atomic orbital (AO) representation, the Fock matrix  $\mathbf{F}$  is composed of a one-electron term  $\mathbf{h}$  and two two-electron terms, the Coulomb ( $\mathbf{J}$ ) and exchange ( $\mathbf{K}$ ) matrices. The latter two arise from contractions between the two-electron repulsion integrals (ERI) and the elements of a given density matrix  $\mathbf{D}$ , viz.,

$$J_{\mu\nu} = \sum_{\lambda\sigma} (\mu\nu|\lambda\sigma) D_{\sigma\lambda}, \quad (1)$$

$$K_{\mu\nu} = \sum_{\lambda\sigma} (\mu\sigma|\lambda\nu) D_{\sigma\lambda}, \quad (2)$$

where the ERIs have been written in the Mulliken notation and the density matrix can be that in Hartree-Fock (HF), Kohn-Sham (KS), or time-dependent density functional (TDDFT)<sup>2</sup> theories. While the ERIs can be evaluated analytically when Gaussian functions are taken as the AOs, the formally quartic scaling places a bottleneck on both computational cost and memory footprint. The very first key for reducing the computational cost and memory requirement is the use of integral upper bounds<sup>3-6</sup> to pre-screen the ERIs on one hand and recalculate them whenever needed on the other hand. Such integral-direct self-consistent field (SCF) has an asymptotically quadratic scaling, due to the fact that the number of numerically significant AO pairs scales linearly with molecular size (characterized by the number of atoms).<sup>7,8</sup> Since the pre-screening tends to pick up different batches of the ERIs for the Coulomb and exchange interactions, it is advantageous to construct them separately to break the quadratic wall.<sup>9</sup> For the former, the resolution of the identity (RI; also called density fitting)<sup>10-17</sup> turns out to be very effective for medium-sized systems (up to a few hundred atoms). Therein, a set of fitting functions is invoked to approximate the AO products, such that the expensive four-center ERIs can be assembled in terms of two- and three-center ERIs. Although the scaling with molecular size is cubic here (due to the matrix inversion needed to

calculate the expansion coefficients), the prefactor is very small. Given well-trained fitting functions,<sup>15,18–20</sup> very high accuracy can be achieved.<sup>15,21,22</sup> Yet, some care should be taken to avoid unphysical situations (e.g., zero or even negative fitted densities) when using the fitting functions optimized for ground state calculations in otherwise excited state calculations.<sup>23,24</sup> Such problems are less prone in the Cholesky decomposition (CD) approach,<sup>25–29</sup> where the fitting functions (Cholesky vectors) are generated on-the-fly with well-controlled accuracy, albeit at the price of some computational overhead. For very large systems, the charge distributions (AO pairs) can be decomposed into overlapping and well-separated ones, thereby splitting the Coulomb potential  $V_c(\vec{r})$  into near- and far-field contributions. Although the former must be calculated directly with the RI/CD-ERIs, the latter can be evaluated by means of multipole expansions,<sup>30–37</sup> thereby achieving a linear-scaling construction of the Coulomb matrix. Since the near-field contributions scale linearly with molecular size (due to the local nature of the basis functions), the linear-scaling construction of the Coulomb matrix can be achieved even for systems with a delocalized electronic structure (i.e., with a non-sparse density matrix).

The situation is different for the exchange matrix: a linear-scaling construction can only be achieved for gapped systems featuring localized electronic structures, because only in such cases the density matrix elements  $D_{\sigma\lambda}$  tend to decay exponentially with respect to spatial separations of the basis functions  $\sigma$  and  $\lambda$ .<sup>38,39</sup> It follows that the four functions in the exchange ERI ( $\mu\sigma|\lambda\nu$ ) must then be close to each other in space to have a significant contribution. Consequently, the number of numerically significant ERIs for the exchange interaction scales linearly with molecular size. However, the pre-screening step still scales quadratically. Several algorithms<sup>39–44</sup> have been designed to resolve this. Yet, their performances deteriorate for extended basis sets (especially in the presence of diffuse functions), due to reduced sparsity of the density matrix. The problem can largely be resolved by introducing an auxiliary density matrix and using a density functional correction for the difference between the true and auxiliary density matrices.<sup>45</sup> The exchange matrix can also be

constructed with the RI/CD techniques<sup>20,29,46,47</sup> but which become effective only with local fittings.<sup>48–53</sup> Moreover, it is possible to further accelerate the construction of the exchange matrix by evaluating a large portion of the exchange ERIs with multipole expansions.<sup>54,55</sup>

Apart from the above analytical evaluations, the Coulomb and exchange matrices can also be constructed semi-numerically<sup>56–62</sup> and even fully numerically.<sup>63–67</sup> Among these, the semi-numerical change-of-spheres algorithm for the exchange build (COSX)<sup>57–60</sup> is particularly advantageous for extended basis sets with functions of high angular momenta and meanwhile has a good balance between performance and accuracy,<sup>68,69</sup> whereas the fully numerical multipole expansion of the Coulomb potential (MECP)<sup>65–67</sup> is most efficient for the Coulomb build, for it is independent of basis set size and electron kinematics (nonrelativistic or relativistic). Yet, the errors resulting from the use of finite grids are often case dependent, which not only affect the calculated energies and gradients, but may also affect iteration processes. This is precisely the issue we want to handle in this work. It will be shown that the evaluation of the  $\mathbf{J}[\mathbf{D}]$  matrix can be facilitated by decomposing the density matrix  $\mathbf{D}$  into three portions, i.e., the superposition of atomic density matrices ( $\mathbf{D}_{\oplus}^A$ ), the portions for near ( $\mathbf{D}^{RC}$ ) and distant ( $\mathbf{D}^{RL} = \mathbf{D}^R - \mathbf{D}^{RC}$ ;  $\mathbf{D}^R = \mathbf{D} - \mathbf{D}_{\oplus}^A$ ) AO pairs, such that  $\mathbf{J}[\mathbf{D}_{\oplus}^A]$  can readily be evaluated analytically, whereas  $\mathbf{J}[\mathbf{D}^{RC}]$  and  $\mathbf{J}[\mathbf{D}^{RL}]$  can be evaluated to sufficient accuracy with semi-numerical integration and MECP, respectively. As a matter of fact, the latter two can be combined (i.e.,  $\mathbf{J}[\mathbf{D}^R]$ ) and evaluated with MECP during the iterations. That is, the separate treatment of  $\mathbf{J}[\mathbf{D}^{RC}]$  and  $\mathbf{J}[\mathbf{D}^{RL}]$  is performed only once upon convergence, so as to avoid repeated evaluations of the relatively expensive  $\mathbf{J}[\mathbf{D}^{RC}]$ . The so-defined hybrid  $\mathbf{J}$ -build is dubbed analytical-MECP (aMECP). Likewise, the analytic evaluation of  $K[\mathbf{D}_{\oplus}^A]$  and semi-numerical evaluation of  $K[\mathbf{D}^R]$  are also invoked for the construction of the exchange matrix  $K[\mathbf{D}]$  during the SCF iterations. The COSX algorithm<sup>57</sup> is employed for  $K[\mathbf{D}^R]$  but with a revised construction of the S-junctions for overlapping AO pairs. To distinguish from the original COSX algorithm (which does not involve the partition of the density matrix  $\mathbf{D}$ ), we denote the presently revised variant as COSx. Upon convergence,

$\mathbf{D}^R$  is further split into re-scaled near ( $\tilde{\mathbf{D}}^{RC}$ ) and distant ( $\tilde{\mathbf{D}}^{RL}$ ) AO pairs. The former is evaluated analytically, whereas the latter is evaluated via COSx. Such a hybrid  $\mathbf{K}$ -build is dubbed ‘analytic-COSx’ (aCOSx). The detail of aMECP and aCOSx will be presented in Sec. 2 and benchmarked in Sec. 4. Some concluding remarks will be provided in Sec. 5 to close the presentation.

## 2 Methodologies

### 2.1 aMECP

For a semi-numerical evaluation of the Coulomb matrix elements, we rewrite Eq. (1) as

$$J_{\mu\nu}[\mathbf{D}] = \int \chi_{\mu}(\vec{r})\chi_{\nu}(\vec{r})V_c[\rho](\vec{r})d^3r \quad (3)$$

$$\approx \sum_g^{N_g} w(\vec{r}_g)\chi_{\mu}(\vec{r}_g)V_c[\rho](\vec{r}_g)\chi_{\nu}(\vec{r}_g), \quad (4)$$

$$V_c[\rho](\vec{r}_g) = \int \frac{\rho(\vec{r})}{|\vec{r}_g - \vec{r}|}d^3r, \quad \rho(\vec{r}) = \sum_{\lambda\sigma} \chi_{\lambda}(\vec{r})\chi_{\sigma}(\vec{r})D_{\sigma\lambda} \quad (5)$$

$$= \sum_{\lambda\sigma} A_{\lambda\sigma}^g D_{\sigma\lambda}, \quad (6)$$

$$A_{\lambda\sigma}^g = \int \frac{\chi_{\lambda}(\vec{r})\chi_{\sigma}(\vec{r})}{|\vec{r}_g - \vec{r}|}d^3r, \quad (7)$$

where  $\{\vec{r}_g\}_{g=1}^{N_g}$  and  $\{w(\vec{r}_g)\}_{g=1}^{N_g}$  represent the integration grid points and corresponding weights, respectively. The  $\mathbf{A}^g$  matrix (7) for each grid point involves 3-center-1-electron (3c1e) Coulomb integrals and can be evaluated analytically in the same way as that for the attraction potential of a nucleus (see Sec. S1 in the Supporting Information for a special treatment of such 3c1e integrals over basis functions of summed angular momenta up to 4). However, since the number of grid points is typically thousands of times the number of atoms, the computational of all  $\mathbf{A}^g$  has a quadratic scaling with a very large prefactor. Here,

we adopt a hybrid analytical-numerical scheme by first decomposing the density matrix as

$$\mathbf{D} = \mathbf{D}_{\oplus}^A + \mathbf{D}^R, \quad \mathbf{D}^R = \mathbf{D}^{RC} + \mathbf{D}^{RL}, \quad (8)$$

and hence the Coulomb matrix as

$$\mathbf{J}[\mathbf{D}] = \mathbf{J}[\mathbf{D}_{\oplus}^A] + \mathbf{J}[\mathbf{D}^R], \quad \mathbf{J}[\mathbf{D}^R] = \mathbf{J}[\mathbf{D}^{RC}] + \mathbf{J}[\mathbf{D}^{RL}]. \quad (9)$$

Here,  $\mathbf{D}_{\oplus}^A$  is the superposition of atomic density matrices obtained from calculations of spherical and unpolarized atomic configurations, and  $\mathbf{D}^{RC}$  represents the portion of  $\mathbf{D}$  for near AO pairs, viz.,

$$D_{\sigma\lambda}^{RC} = \begin{cases} D_{\sigma\lambda}^R & [R_{\sigma\lambda} < R_{\sigma}^{cut} + R_{\lambda}^{cut}] \cap [D_{\sigma\lambda}^R > \eta_D] \\ 0 & [R_{\sigma\lambda} \geq R_{\sigma}^{cut} + R_{\lambda}^{cut}] \cap [D_{\sigma\lambda}^R \leq \eta_D], \end{cases} \quad (10)$$

where  $\eta_D$  ( $= 10^{-8}$ ) is a predefined threshold,  $R_{\sigma\lambda}$  is the distance between atomic centers of two primitive Gaussian functions  $\chi_{\sigma}$  and  $\chi_{\lambda}$ , whereas the cutoff radius  $R_{\sigma}^{cut}$  of function  $\chi_{\sigma}$  is determined by the following radial integration

$$\int_{r=R_{\sigma}^{cut}}^{\infty} R_{\sigma}^2(r) r^2 dr = \eta_b. \quad (11)$$

in which  $R_{\sigma}(r)$  is the radial part of a primitive GTO. The parameter  $\eta_b$  is usually to be set to 0.30 in energy calculations but to 0.35 in gradient calculations. Although the semi-numerical evaluation of  $\mathbf{J}[\mathbf{D}^{RC}]$  (cf. Eqs. (4) and (6)) has a quadratic scaling, the band structure of  $\mathbf{D}^{RC}$  ensures a small prefactor. This holds also for the analytical evaluation of  $\mathbf{J}[\mathbf{D}_{\oplus}^A]$  due to the diagonal-in-atom structure of  $\mathbf{D}_{\oplus}^A$ . In particular, thanks to the spherical averaging, each atomic density matrix has vanishing elements between basis functions of different angular momenta and between functions that have no contributions to the occupied atomic orbitals. As for the potential due to the residual density matrix  $\mathbf{D}^{RL}$ , which is small in magnitude but

may spread over the whole system, we adopt the MECP approach,<sup>65-67</sup> where the residual density  $\rho^{RL}(\vec{r})$  is first partitioned into a sum of one-centered contributions via a normalized partition function,<sup>70</sup>

$$\rho^{RL}(\vec{r}) = \sum_{\lambda\sigma} \chi_\lambda(\vec{r})\chi_\sigma(\vec{r})D_{\sigma\lambda}^{RL} = \sum_A P_A(\vec{r})\rho^{RL}(\vec{r}) = \sum_A \rho_A^{RL}(\vec{r}). \quad (12)$$

The one-centered densities are then projected onto their multipole components,

$$\rho_{Alm}^{RL}(r_A) = \int_{|\vec{r}-\vec{R}_A|=r_A} Y_{lm}(\hat{r}_A)\rho_A^{RL}(\vec{r})d\Omega, \quad r_A = |\vec{r}-\vec{R}_A|, \quad (13)$$

so as to approximate the residual density as

$$\rho^{RL}(\vec{r}) = \sum_A \sum_{l=0}^{L_{\max}} \sum_{m=-l}^l Y_{lm}(\hat{r}_A)\rho_{Alm}^{RL}(r_A). \quad (14)$$

Further using the multipole expansion of  $1/|\vec{r}_1-\vec{r}_2|$ , the Coulomb potential can be calculated as

$$V_c[\rho^{RL}](\vec{r}) = \sum_A \sum_{l=0}^{L_{\max}} \sum_{m=-l}^l \frac{4\pi}{2l+1} Y_{lm}(\hat{r}_A)V_{Alm}^{RL}(r_A), \quad (15)$$

$$V_{Alm}^{RL}(r_A) = \frac{1}{r_A^{l+1}} \int_0^{r_A} \rho_{Alm}^{RL}(s)s^{l+2}ds + r_A^l \int_{r_A}^\infty \rho_{Alm}^{RL}(s)s^{1-l}ds. \quad (16)$$

To facilitate the calculations of the right hand sides of Eqs. (16) and (15), the tabulated  $r_A^2\rho_{Alm}^{RL}(r_A)$  and  $V_{Alm}^{RL}(r_A)$  are fitted with cubic splines. Plugging  $V_c[\rho^{RL}](\vec{r}_g)$  into Eq. (4) gives rise to  $J_{\mu\nu}[\mathbf{D}^{RL}]$ . Eqs. (12)-(14) and (16) all scale linearly, but Eq. (15) scales quadratically with molecular size. However, the prefactor of the latter is very small, due to the short-range nature of the numerical functions  $\{V_{Alm}^{RL}(\cdot)\}$  for angular momenta higher than 2. Compared to other density fitting approaches,<sup>10-17</sup> the MECP scheme amounts to using saturated fitting functions of angular momenta up to  $L_{\max}$ , but without explicit fitting functions. It also deserves to be mentioned that the present extraction of  $\mathbf{D}_\oplus^A$  from the full density matrix  $\mathbf{D}$  is

more natural and more accurate than the introduction<sup>64</sup> of a crude model density matrix for the purpose of curing the numerical errors arising from the long-range part of the numerically evaluated Coulomb potential.<sup>63</sup>

As a matter of fact, the relatively expensive semi-numerical evaluation of  $\mathbf{J}[\mathbf{D}^{RC}]$  (10) need not be performed in each SCF iteration. Instead, the use of MECP for  $\mathbf{J}[\mathbf{D} - \mathbf{D}_{\oplus}^A]$  is sufficient during the iterations. As such, the separate treatment of  $\mathbf{J}[\mathbf{D}^{RC}]$  and  $\mathbf{J}[\mathbf{D}^{RL}]$  needs to be performed only once in the end of iterations, which is necessary to ensure the accuracy. It also deserves to be mentioned that MECP itself is sufficiently accurate for the induced Coulomb potential entering TDDFT calculations.

## 2.2 aCOSx

For a semi-numerical evaluation of the exchange matrix, Eq. (2) can be rewritten as<sup>57</sup>

$$K_{\mu\nu} \approx \frac{1}{2}(\tilde{K}_{\mu\nu} + \tilde{K}_{\nu\mu}), \quad (17)$$

$$\tilde{K}_{\mu\nu} = \sum_g^{N_g} w(\vec{r}_g) \chi_\mu(\vec{r}_g) \chi_\nu(\vec{r}_g) A_{\lambda\nu}^g D_{\sigma\lambda} = (\mathbf{X}\mathbf{G}^\dagger)_{\mu\nu}, \quad (18)$$

$$X_{\mu g} = w_g^{1/2} \chi_\mu(\vec{r}_g), \quad F_{\lambda g} = (\mathbf{D}\mathbf{X})_{\lambda g}, \quad G_{\nu g} = \sum_\lambda A_{\nu\lambda}^g F_{\lambda g}. \quad (19)$$

It can be shown<sup>57</sup> that even the steepest scaling intermediate  $G_{\nu g}$  has a very favourable scaling with the maximum angular momentum in the basis set, as compared with the analytical evaluation of  $K_{\mu\nu}$ . The numerical accuracy can further be improved by means of the overlap fitting,<sup>58</sup>

$$\mathbf{K} \approx \frac{1}{2}(\mathbf{S}\mathbf{S}_{\text{num}}^{-1}\tilde{\mathbf{K}} + c.c.), \quad (20)$$

where  $\mathbf{S}$  and  $\mathbf{S}_{\text{num}}$  ( $= \mathbf{X}\mathbf{X}^\dagger$ ) are the overlap matrices calculated analytically and numerically, respectively.

For an efficient implementation of the above scheme, the COSX algorithm<sup>57</sup> first determines the radial extension of each shell of contracted basis functions and then establishes a list of partners (S-junction) for each basis function according to an overlap criterion. A second list of partners (P-junction) is further constructed for each basis function according to a cutoff criterion for the density matrix elements. The length of the S-junction for every basis function approaches constant due to the short-range nature of the basis function, whereas the length of the P-junction is determined by the degree of localization of the electronic structure (i.e., sparsity of the density matrix). Pictorially, two basis functions  $\chi_\mu$  and  $\chi_\nu$  are confined in their spheres  $\mathcal{S}_\mu$  and  $\mathcal{S}_\nu$ , respectively, which are connected to a number of spheres  $\{\mathcal{S}_\sigma\}$  of  $\{\chi_\sigma\}$  and  $\{\mathcal{S}_\lambda\}$  of  $\{\chi_\lambda\}$ , respectively. The latter spheres are further connected, thereby forming chains of (atom-centered and connected) spheres for the basis pair  $\chi_\mu\chi_\nu$  in the exchange ERIs ( $\mu\sigma|\lambda\nu$ ). In the aCOSx approach presented here, instead of determining the radial extensions of shells of *contracted* basis functions according to their absolute values in a point-wise manner, the radial extensions  $\{R_\mu\}$  of *primitive* basis functions  $\{\chi_\mu\}$  are estimated simply according to the integral defined in Eq. (11) with  $\eta_b = 0.001$ . Two primitive functions  $\chi_\mu$  ( $\chi_\nu$ ) and  $\chi_\sigma$  ( $\chi_\lambda$ ) are connected if the sum of their radii is smaller than the distance between the atoms to which they belong. The functions  $\chi_\sigma$  and  $\chi_\lambda$  in the exchange ERIs ( $\mu\sigma|\lambda\nu$ ) are regarded as connected only if the density matrix element  $D_{\sigma\lambda}$  is larger than a preset threshold  $\delta_D$  ( $= 10^{-8}$ ). Numerical experimentations reveal that the aCOSx is more effective than the original COSX in reducing the number of numerically significant 3c1e integrals  $A_{\lambda\nu}^g$ , albeit with a somewhat larger memory requirement.

The number of grid points is a crucial factor for the efficiency of aCOSx. After extensive experimentations, we propose the following rule for the number of Gauss-Chebyshev type of radial grid points,

$$N_R(r, Z, K, L) = 5r + N_q(Z) + 5K + 15L, \quad K, L \in [0, 9], \quad (21)$$

where  $r$  is the row of the period table to which the atom belongs, whereas  $N_q$  is function of nuclear charge  $Z$  (see Table 1). Since it is natural<sup>71</sup> to use different Lebedev angular grids<sup>72,73</sup> for different regions in space, the atomic radius  $R$  is decomposed into seven intervals  $[a_{i-1}R, a_iR)$ , with  $a_0 = 0$  and  $a_i$  ( $i \in [1, 6]$ ) given in Table 2. The numbers of angular grid points for different radial intervals are controlled by the parameter  $M + \Delta M$ :  $M$  ( $\geq 1$ ) in Table 3 tells the number of angular grid points for the fourth interval  $[a_3R, a_4R)$ , whereas  $\Delta M$  in Table 4 tells the reduced number of angular grid points for other intervals. Overall, the size of the grid in the aCOSx calculations can be characterized by function  $G_{KLM}$ . For instances,  $G_{002}$  is typically used in SCF and TDDFT calculations. The so-generated grids are finally pruned.<sup>74,75</sup>

**Table 1: Function  $N_q(Z)$  in Eq. (21)**

atom	H-Ne	Na-Kr	Rb-Xe	Cs-Yb	Lu-Hg	Tl-
$N_q(Z)$	10	15	20	25	30	40

**Table 2: Parameters for defining radial intervals  $[a_{i-1}R, a_iR)$  ( $a_0 = 0$ )**

atom	$a_i$					
	$a_1$	$a_2$	$a_3$	$a_4$	$a_5$	$a_6$
H-He	0.25	0.50	1.00	4.50	7.80	10.00
Li-Ne	0.17	0.50	0.90	3.50	7.80	9.00
Na-Ar	0.10	0.40	0.80	2.50	5.00	7.50
K-	0.02	0.10	0.20	3.50	7.00	9.00

**Table 3: Correspondence between  $M$  in  $G_{KLM}$  and number of Lebedev angular grids**

atom	$M$													
	-4	-3	-2	-1	0	1	2	3	4	5	6	7	8	9
H -Pd	6	6	6	14	26	38	50	110	194	302	434	590	770	974
Ag-Yb	6	6	14	26	38	50	110	194	302	434	590	770	974	1202
Lu-	6	14	26	38	50	110	194	302	434	590	770	974	1202	1454

Another feature of the present aCOSx lies in that, like in aMECP, the density matrix  $\mathbf{D}$

**Table 4: Parameter  $\Delta M$  for adjusting the number of Lebedev angular grids**

interval	$[0, a_1R)$	$[a_1R, a_2R)$	$[a_2R, a_3R)$	$[a_3R, a_4R)$	$[a_4R, a_5R)$	$[a_5R, a_6R)$	$[a_6R, \infty)$
$\Delta M$	-3	-2	-1	0	-1	-3	-5

is decomposed as

$$\mathbf{D} = \mathbf{D}_{\oplus}^A + \mathbf{D}^R, \quad (22)$$

such that the exchange matrix is decomposed as

$$\mathbf{K}[\mathbf{D}] = \mathbf{K}[\mathbf{D}_{\oplus}^A] + \mathbf{K}[\mathbf{D}^R], \quad (23)$$

where  $\mathbf{K}[\mathbf{D}_{\oplus}^A]$  needs to be calculated analytically only once, whereas  $\mathbf{K}[\mathbf{D}^R]$  is updated semi-numerically during the iterations with a smaller grid  $G_{KLM}$ . After convergence of the SCF iterations, the  $D^R$  is first decomposed as

$$\mathbf{D}^R = \mathbf{D}^{RC} + \mathbf{D}^{RL}, \quad (24)$$

where

$$D_{\mu\nu}^{RC} = \begin{cases} D_{\mu\nu}^R & [R_{\mu\nu} \leq R_{\mu}^{cut} + R_{\nu}^{cut}] \cap [L(\chi_p) \leq L_{OMax}^A(\chi_p), \quad p \in \mu, \nu], \\ 0. & \end{cases} \quad (25)$$

Here,  $R_{\mu}^{cut}$  is the cutoff radius of a primitive basis function  $\chi_{\mu}$  as defined in Eqn. 11.  $L(\chi_p)$  represents the orbital angular momentum of a basis function  $\chi_p$ , and  $L_{OMax}^A(\chi_p)$  signifies the maximum angular momentum of the occupied orbital of the atom A to which  $\chi_p$  is associated.

Then,  $\mathbf{D}^{RC}$  and  $\mathbf{D}^{RL}$  are re-scaled as

$$\tilde{\mathbf{D}}^{RC} = \mathbf{D}^{RC} + \frac{n^{RL}}{n^A} \mathbf{D}_{\oplus}^A, \quad (26)$$

$$\tilde{\mathbf{D}}^{RL} = \mathbf{D}^{RL} - \frac{n^{RL}}{n^A} \mathbf{D}_{\oplus}^A, \quad (27)$$

where

$$n^{RL} = \text{tr}[\mathbf{D}^{RL}\mathbf{S}], \quad n^A = \text{tr}[\mathbf{D}_{\oplus}^A\mathbf{S}], \quad (28)$$

so as to render  $\text{tr}[\tilde{\mathbf{D}}^{RL}\mathbf{S}] = 0$ , meaning that the distant AO pairs do not carry on net electrons. Finally,  $\mathbf{K}[D^R]$  is calculated according to

$$\mathbf{K}[\mathbf{D}^R] = \mathbf{K}[\tilde{\mathbf{D}}^{RC}] + \mathbf{K}[\tilde{\mathbf{D}}^{RL}], \quad (29)$$

where the first term is calculated analytically, whereas the second term is calculated by COSx with a larger grid with  $K + 2$  and  $M + 1$ . We will see in the benchmark calculations that the aCOSx approach defined by Eqs. (23) and (29) is more stable in accuracy than the original algorithm.<sup>57–59</sup>

### 3 Computational details

To expedite subsequent discussions, ERIJ and ERIK are used to denote analytical evaluation of the full  $\mathbf{J}[\mathbf{D}]$  and  $\mathbf{K}[\mathbf{D}]$  matrices, respectively. MECP refers to analytic evaluation of  $\mathbf{J}[\mathbf{D}_{\oplus}^A]$  and numerical evaluation of  $\mathbf{J}[\mathbf{D} - \mathbf{D}_{\oplus}^A]$ , whereas COSx refers here to analytic evaluation of  $\mathbf{K}[\mathbf{D}_{\oplus}^A]$  and semi-numerical evaluation of  $\mathbf{K}[\mathbf{D} - \mathbf{D}_{\oplus}^A]$  with the present construction of S-junctions. aMECP amounts to updating the  $\mathbf{J}[\mathbf{D}^{RC}]$  portion [see Eq. (10)] of  $\mathbf{J}[\mathbf{D} - \mathbf{D}_{\oplus}^A]$  with semi-numerical integration upon convergence of the SCF iterations. Similarly, aCOSx amounts to updating the  $\mathbf{K}[\tilde{\mathbf{D}}^{RC}]$  portion [see Eq. (26)] of  $\mathbf{K}[\mathbf{D} - \mathbf{D}_{\oplus}^A]$  with analytic inte-

gration upon convergence of the SCF iterations. While MECP and aMECP can adopt the same medium, fine or ultra-fine grids<sup>76</sup> as used in density functional calculations, COSx and aCOSx will adopt the  $G_{002}$ ,  $G_{003}$ , and  $G_{013}$  grids as described in Sec. 2.2. Additional computational details will be exposed along with the presentation of the results. All calculations were performed with the BDF program package.<sup>66,67,77,78</sup>

## 4 Results and discussion

To reveal the performances of the (a)MECP and (a)COSx algorithms, four algorithmic combinations, i.e., MECP+ERIK, aMECP+ERIK, ERIJ+COSx, and ERIJ+aCOSx, are first compared with ERIJK for the Hartree-Fock (HF) total energies of 20 molecules (denoted as Mole20) with the cc-pVDZ basis sets.<sup>79</sup> The Mole20 set includes 10 pharmaceutical molecules of the benchmark set used by Neese to access the COSX algorithm<sup>57</sup> and the following 10 molecules: two water clusters ( $(\text{H}_2\text{O})_{18}$  and Icecube27), a DNA molecule,  $\text{C}_{60}$ , a carbon nanotube (CNT40), beta-carotene, a bacteria-chromophore molecule (Bacl), a thermally activated delayed fluorescence molecule (TADFmol), the (amylose)<sub>4</sub> chain, and olestra. Their Cartesian coordinates are provided in the Supporting Information. The mean absolute errors (MAE) and maximum absolute errors (MaxAE) of the methods are depicted in Fig. 1a and 1b, respectively (see Tables S1 and S2 in the Supporting Information for more details). It can be seen that, when the medium grid is employed in MECP, MECP+ERIK has a substantial MAE of 77.69  $\mu\text{E}_h/\text{atom}$ , which is accompanied by a MaxAE of 721.72  $\mu\text{E}_h/\text{atom}$ . When the fine grid is used, both the MAE and MaxAE are reduced but which cannot further be reduced with increased grid size. In contrast, the MAE of aMECP+ERIK falls below 1  $\mu\text{E}_h/\text{atom}$  and is not sensitive to grid sizes (e.g., 0.23, 0.15, and 0.16  $\mu\text{E}_h/\text{atom}$  for the medium, fine, and ultra-fine grids, respectively), thereby demonstrating the superiority of aMECP over MECP. It is noteworthy that the MaxAEs of aMECP+ERIK utilizing the three different grids are also below 1  $\mu\text{E}_h/\text{atom}$ , signifying the robustness of aMECP in

accuracy.

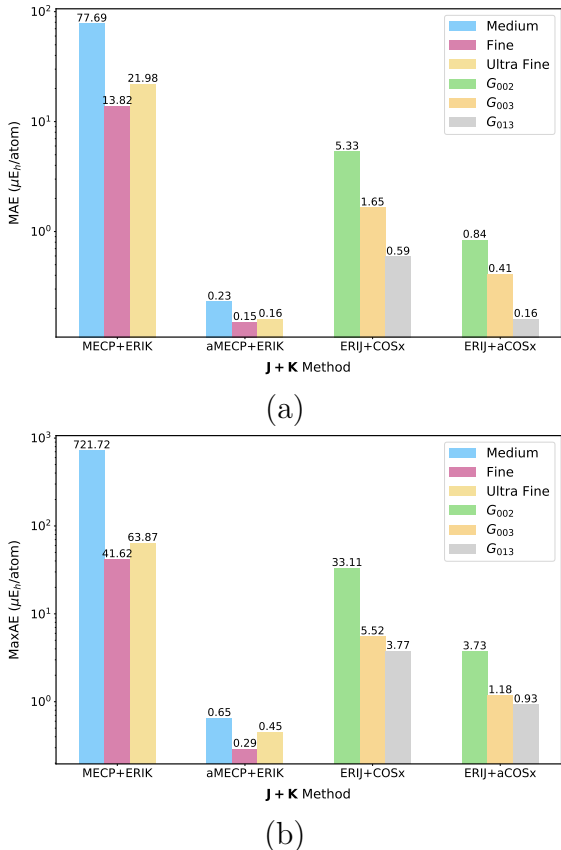


Figure 1: Errors of the MECP+ERIK, aMECP+ERIK, ERIJ+COSx, and ERIJ+aCOSx algorithms for the HF/cc-pVDZ total energies of Mole20. MAE: mean absolute error; MaxAE: maximum absolute error.

The errors of COSx and aCOSx can be revealed by comparing ERIJ+COSx and ERIJ+aCOSx with ERIJK. It can be seen from Fig. 1a and 1b that the MAE of ERIJ+COSx with the small grid  $G_{002}$  is  $5.33 \mu E_h/\text{atom}$ , while the MaxAE reaches  $33.11 \mu E_h/\text{atom}$ . Increasing the grid from  $G_{002}$  to  $G_{003}$  does reduce the error of COSx but at the expense of an increased computational cost. In contrast, even with the small grid  $G_{002}$ , the MAE of aCOSx is already below  $1 \mu E_h/\text{atom}$ . In particular, its MaxAE is only  $3.22 \mu E_h/\text{atom}$ , an order of magnitude lower than that of COSx.

Now the question is how the combination of aMECP and aCOSx performs. It is known from Fig. 1 that the error of aCOSx tends to be somewhat larger than that of aMECP for the Mole20 benchmark set. It can hence be anticipated that the MAE of aMECP+aCOSx

is dominated by that of aCOSx. The latter should decrease for hybrid functionals with less exact exchange. To confirm this, we took M06-HF,<sup>80</sup> seven hybrid functionals (M06-2X,<sup>81</sup> Cam-B3LYP,<sup>82</sup> PBE38,<sup>83</sup> PBE0,<sup>84</sup> B3LYP,<sup>85,86</sup> and TPSSh<sup>87</sup>), and one pure density functional (PBE<sup>88</sup>), which have decreasing percentage of exact exchange. All these functionals were implemented by using libxc.<sup>89</sup> The basis sets were def2-TZVP.<sup>19</sup> As can be seen from Fig. 2, the MAEs of aMECP+aCOSx do decrease as decrease of the amount of exact exchange.

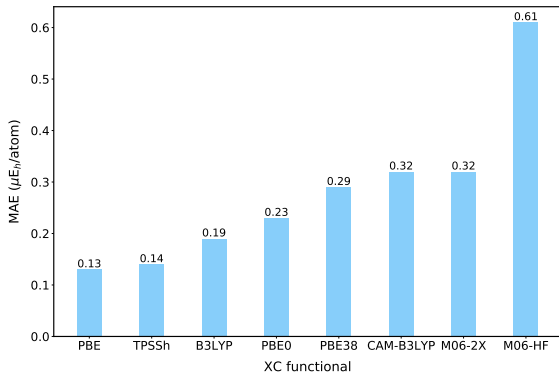


Figure 2: Mean absolute errors (MAE) of DFT calculations of Mole20 with aMECP+aCOSx and different functionals.

To have a more extensive examination of the aMECP+aCOSx-HF algorithm, we took 1210 molecules from the ACCDB database<sup>90</sup> (see the Supporting Information for more details). The medium grid and the  $G_{002}$  grid were used for aMECP and aCOSx, respectively. To check possible basis set dependence, three basis sets (def2-SVP, def2-TVZP, and def2-QVZP<sup>19</sup>) were employed. The distributions of the energy errors as well as the MAEs for aMECP+ERIK, ERIJ+aCOSx, aMECP+aCOSx are illustrated in Fig. 3. It can be seen that aMECP+aCOSx is insensitive to basis sets, with the MAEs all below  $1 \mu E_h/\text{atom}$ . Therefore, aMECP+aCOSx can be recommended as an efficient Fock build in HF and DFT calculations.

The accuracy of aMECP+aCOSx should be even higher for relative energies. To see this, we calculated the isomerization energies ( $E_{\text{iso}}$ ) of ISOL24<sup>91</sup> and reaction barriers ( $E_{\text{bar}}$ ) of a subset of INV24.<sup>92</sup> Again, the medium grid and the  $G_{002}$  grid were used for aMECP and

aCOSx, respectively, in conjunction with B3LYP/def2-TZVP. The results are documented in Tables 5 and 6, respectively. It can be seen that the MaxAEs of aMECP+aCOSx for  $E_{\text{iso}}$  and  $E_{\text{bar}}$  are only 0.022 and 0.056 kcal/mol, respectively.

MECP was known to be very accurate for TDDFT excitation energies.<sup>24,93,94</sup> The question is how COSx performs in TDDFT calculations. To see this, we calculated 10 lowest singlet excited states for each molecule of the Mole20 set with MECP (medium grid) and COSx ( $G_{002}$  grid), in conjunction with PBE0/cc-pVDZ. The SCF calculations were performed by using aMECP+aCOSx. As can be seen from Fig. 4, compared with the ERIJK-TDDFT calculations, the errors of the MECP+COSx-TDDFT excitation energies are typically within the range of -0.002 to 0.002 eV. Only four of the 200 excited states have errors somewhat larger than 0.002 eV, with the largest error being 0.004 eV. Moreover, the oscillator strengths calculated by MECP+COSx are also very close to those by the ERIJK-TDDFT calculations (see Table S3 in the Supporting Information). Therefore, MECP+COSx can safely be used in TDDFT calculations after SCF calculations with aMECP+aCOSx.

Having determined the accuracy of the aMECP+aCOSx and MECP+COSx algorithms for SCF and TDDFT calculations, respectively, it is time to check their speedups over ERIJK. It can be seen from Fig. 5 that the aMECP+aCOSx and MECP+COSx algorithms have achieved remarkable accelerations even for the smallest molecule, Adinane composed only of 15 atoms. The calculations with pure density functionals (e.g., BLYP) exhibit a more pronounced speedup over those with hybrid functionals (e.g., B3LYP). This is not surprising, for the former involve only Coulomb-type ERIs. It is more gratifying to see that the fewer the hydrogen atoms, the larger the speedup (e.g, CNT40 and C60), and the more extended the basis set, the larger the speedup (e.g., the average speedups of 3.11 (SCF) and 4.70 (TDDFT) with cc-pVDZ vs. 6.54 (SCF) and 15.62 (TDDFT) with cc-pVTZ).

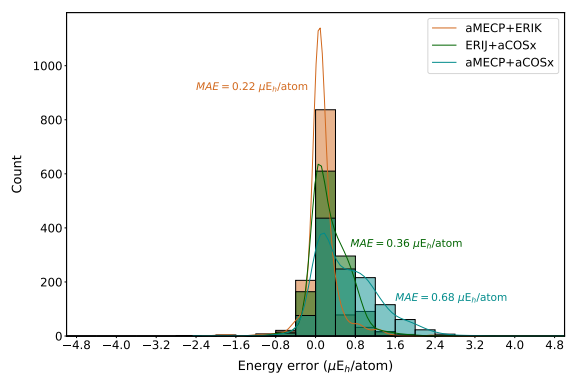
Finally, the timings and scalings of the  $\mathbf{J}[\mathbf{D}_{\oplus}^A]$ ,  $\mathbf{J}[\mathbf{D}^R]$ , and  $\mathbf{J}[\mathbf{D}^{RC}]$  and  $\mathbf{J}[\mathbf{D}^{RL}]$  terms in aMECP as well as the  $\mathbf{K}[\mathbf{D}_{\oplus}^A]$ ,  $\mathbf{K}[\mathbf{D}^R]$ ,  $\mathbf{K}[\tilde{\mathbf{D}}^{RL}]$ , and  $\mathbf{K}[\tilde{\mathbf{D}}^{RC}]$  terms in aCOSx are shown in Fig. 6. The HF/def2-TVZP calculations were performed for the N-amylose chains ( $N =$

2, 4, 8, 16). As can be seen from Fig. 6(a), the  $\mathbf{J}[\mathbf{D}_{\oplus}^A]$ ,  $\mathbf{J}[\mathbf{D}^R]$  and  $\mathbf{J}[\mathbf{D}^{RL}]$  terms are very cheap, whereas the  $\mathbf{J}[\mathbf{D}^{RC}]$  term consumes about 80% of the aMECP runtime, although it is evaluated semi-numerically only once. The most expensive quantity,  $A_{\lambda\mu}^g$  (7), involved in  $\mathbf{J}[\mathbf{D}^{RC}]$  scales formally as  $O(N_B^3)$  but actually as  $O(N_B^{2.004})$ , due to the fact that the number of AO pairs scales linearly with respect to the molecular size (measured by the number ( $N_B$ ) of basis functions). As a result, the overall scaling of aMECP amounts to  $O(N_B^{1.976})$ . For comparison, the overall scaling of aCOSx,  $O(N_B^{1.518})$ , is somewhat lower. Among the terms in aCOSx,  $\mathbf{K}[\mathbf{D}^R]$  is most expensive ( $O(N_B^{1.563})$ ) during the SCF iterations, which is followed by the one-step  $\mathbf{K}[\tilde{\mathbf{D}}^{RL}]$  ( $O(N_B^{1.726})$ ) and  $\mathbf{K}[\tilde{\mathbf{D}}^{RC}]$  ( $O(N_B^{1.200})$ ) in the end of SCF iterations. In particular, the near-linear scaling term  $\mathbf{K}[\tilde{\mathbf{D}}^{RC}]$  is highly recommended, for it improves the accuracy of COSx significantly.

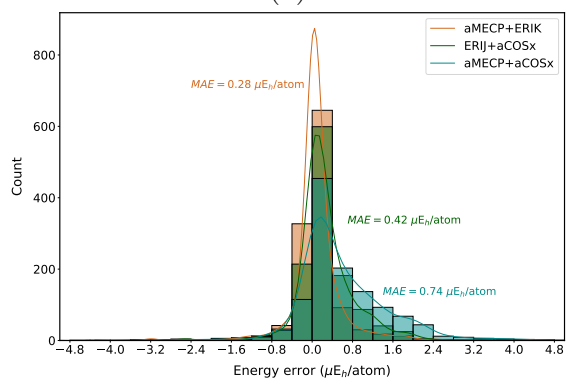
In sum, the aMECP+aCOSx/MECP+COSx algorithm proposed here is highly robust and highly efficient in SCF/TDDFT calculations, particularly when extended basis sets are to be used.

## 5 Conclusion

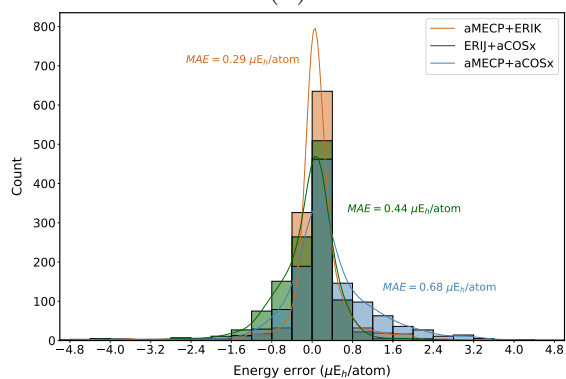
A very robust and efficient hybrid analytic-numerical Fock build, aMECP+aCOSx, has been developed for accelerating HF/DFT calculations. The essential idea is to extract those portions of the Fock matrix (i.e., those corresponding to the superposition of atomic density matrices and the density matrix spanned by the near AO pairs) that can readily be evaluated analytically, so as to minimize numerical noises arising from the semi-numerical and numerical integrations. As a result, the combination of aMECP with a medium grid as used in DFT calculations and aCOSx with a coarse grid ( $G_{002}$ ) is already sufficient to achieve an accuracy of less than  $1 \mu\text{E}_h/\text{atom}$  in total energies. The acceleration of aMECP+aCOSx over the analytic Fock build is already seen in calculations of small molecular systems and is more enhanced in calculations of large molecules with extended basis sets. In contrast,



(a)



(b)



(c)

Figure 3: Distributions of energy errors as well as mean absolute errors (MAE) of aMECP+aCOSx, aMECP+ERIK, and ERJ+aCOSx in HF calculations of 1210 molecules. (a) def2-SVP; (b) def2-TZVP; (c) def2-QZVP.

Table 5: Isomerization energies ( $E_{\text{iso}}$  in kcal/mol) of ISOL24<sup>91</sup> calculated by B3LYP/def2-TVZP with ERIJK and aMECP+aCOSx.

Molecule	Natom	$E_{\text{iso}}$ <sup>a</sup>	$\Delta E_{\text{iso}}$ <sup>b</sup>
i1	72	-75.182	0.007
i2	41	-17.250	0.001
i3	24	-6.844	-0.001
i4	81	-18.184	0.015
i5	32	-21.964	-0.004
i6	48	-22.700	0.008
i7	51	-6.192	-0.003
i8	43	-51.278	0.016
i9	32	-17.832	-0.003
i10	35	-2.027	0.003
i11	30	-36.955	-0.004
i12	40	-0.570	-0.004
i13	26	-29.284	-0.003
i14	26	-2.978	0.001
i15	42	1.785	-0.004
i16	51	-23.579	0.013
i17	44	1.813	0.022
i18	39	-12.612	0.004
i19	36	-20.941	-0.013
i20	28	-4.613	0.014
i21	36	4.243	-0.019
i22	44	16.745	0.013
i23	39	45.483	0.003
i24	52	-7.354	-0.001
MAE			0.007
MaxAE			0.022

<sup>a</sup> Calculated by ERIJK.

<sup>b</sup> Deviations of aMECP+aCOSx from ERIJK.

**Table 6: Reaction barriers ( $E_{\text{bar}}$  in kcal/mol) of the INV24 subset<sup>92</sup> calculated by B3LYP/def2-TVZP with ERIJK and aMECP+aCOSx.**

Molecule	Natom	$E_{\text{bar}}$ <sup>a</sup>	$\Delta E_{\text{bar}}$ <sup>b</sup>
BNCorannulene	30	5.073	0.000
BNSumanene	33	24.325	0.000
Corannulene	30	9.917	0.005
Dibenzocarbazole	34	3.254	-0.001
Dibenzocycloheptene	27	9.087	-0.005
Hexahelicene	42	35.597	0.037
Methinecyanine	40	12.042	0.007
Pentahelicene	36	23.297	-0.006
Ph3	34	24.939	-0.024
Sumanene	33	18.342	-0.019
Tetrabenzopyracylene	38	6.561	0.056
Tetrahelicene	30	3.829	0.006
Triazasumanene	30	38.482	0.009
Triindenotriphenylene	42	65.273	0.017
MAE			0.014
MaxAE			0.056

<sup>a</sup> Calculated by ERIJK.

<sup>b</sup> Deviations of aMECP+aCOSx from ERIJK.

the combination of MECP (with a medium grid) and COSx (with a coarse grid), where only the part of the Fock matrix corresponding to the superposition of atomic density matrices is treated analytically, is already accurate enough for TDDFT calculations of excitation energies and oscillator strengths, for a good reason: it is the orbital products instead of individual orbitals that are the actual basis in TDDFT (and any post-SCF) calculations. Both aMECP+aCOSx and MECP+COSx can readily be extended to the relativistic domain, where the acceleration is expected to be even higher. But before doing this, the GPU implementation should first be finished. Work along these directions is being carried out at our laboratory.

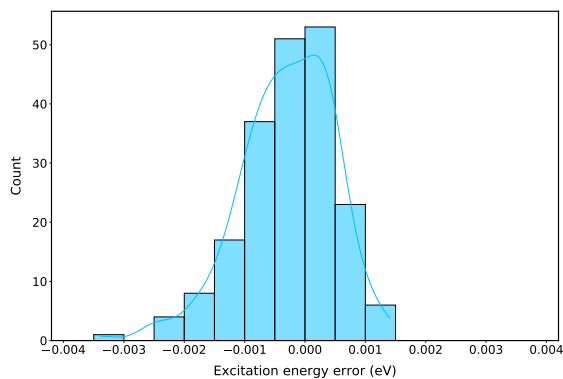


Figure 4: Histogram of errors for 200 TDDFT excitation energies with MECP+COSx.

## Supporting Information Available

Formulas for the three-center-one-electron Coulomb integrals are first presented in Sec. S1. The errors of the aMECP+aCOSx algorithm for the HF energies of the Mole20 set are documented in Tables S1 and S2, whereas the corresponding errors of the MECP+COSx algorithm for the TDDFT excitation energies and oscillator strengths are documented in Table S3. Benchmark sets used to assess aMPEC+aCOSx-HF with different basis sets are described in Sec. S4. The Cartesian coordinates of the Mole20 set are compiled in the file Mole20Coordinates.zip.

## Acknowledgement

The research of this work was supported by National Natural Science Foundation of China (Project Nos. 22373057 and 21873077), Mount Tai Climbing Program of Shandong Province, and Double First-class University Construction Project of Northwest University.

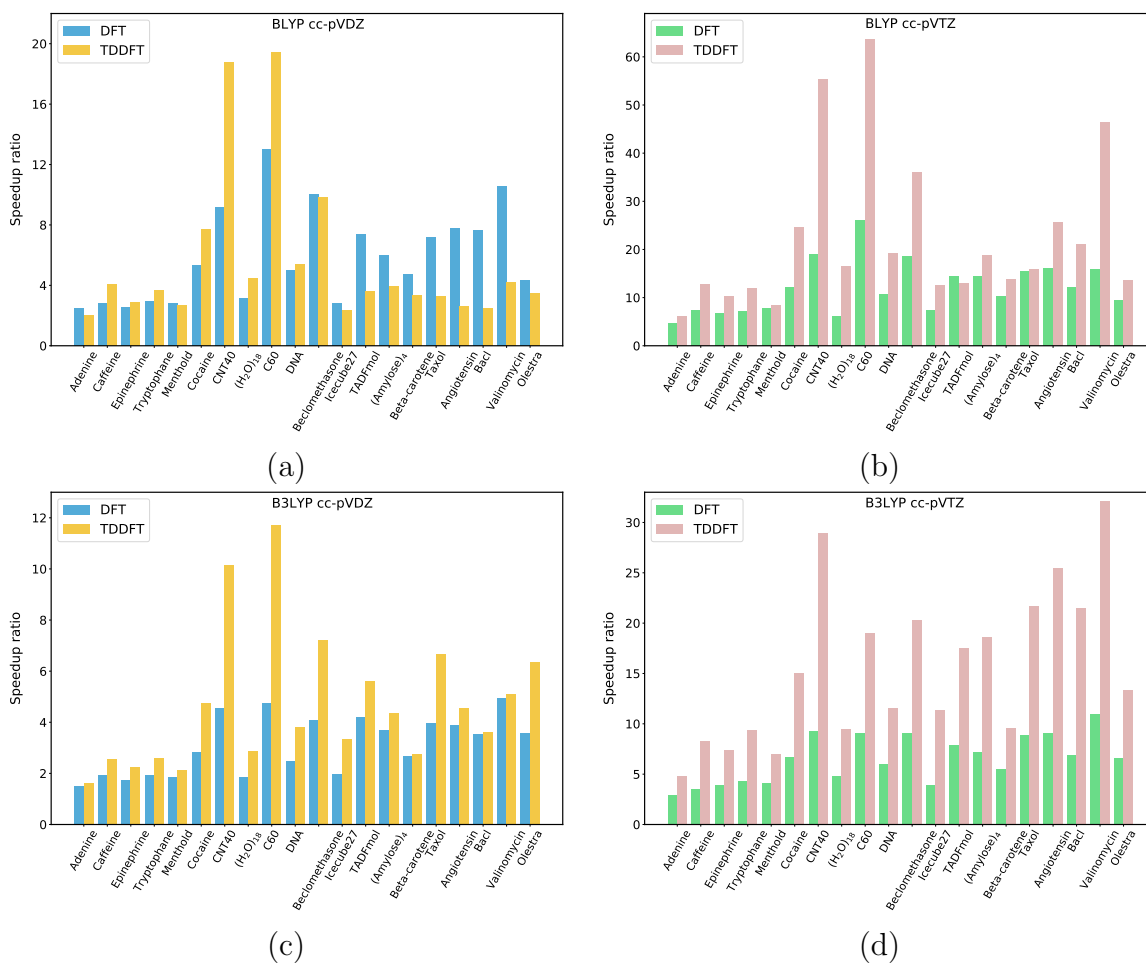
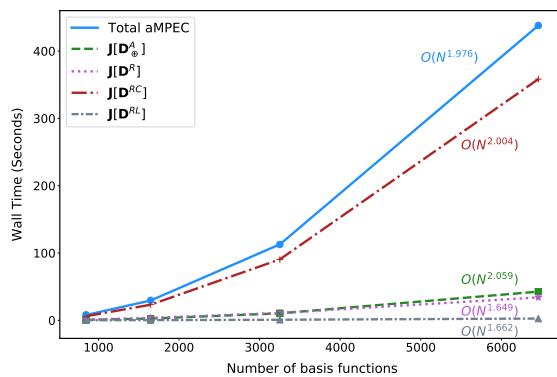
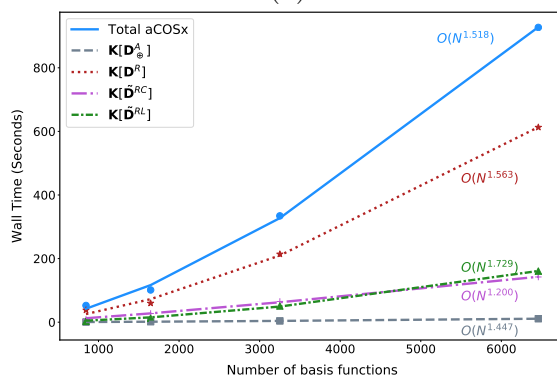


Figure 5: Speedups of (a)MECP+(a)COSx(e) over ERIJK in calculations of SCF energies and TDDFT excitation energies of Mole20. (a) BLYP/cc-pVDZ; (b) BLYP/cc-pVTZ; (c) B3LYP/cc-pVDZ; (d) B3LYP/cc-pVTZ.



(a)



(b)

Figure 6: Timings and scalings of aMECP+aCOSx-HF calculations of N-amylose chains, with 32 OpenMP threads on a computer equipped with an AMD 5975WX CPU and 64G memory.

## References

- (1) Kussmann, J.; Beer, M.; Ochsenfeld, C. Linear-scaling self-consistent field methods for large molecules. *WIREs: Comput. Mol. Sci.* **2013**, *3*, 614–636.
- (2) Casida, M. E. Time-dependent density-functional theory for molecules and molecular solids. *J. Mol. Struct.: THEOCHEM* **2009**, *914*, 3–18.
- (3) Whitten, J. L. Coulombic potential energy integrals and approximations. *J. Chem. Phys.* **1973**, *58*, 4496–4501.
- (4) Gill, P. M.; Johnson, B. G.; Pople, J. A. A simple yet powerful upper bound for Coulomb integrals. *Chem. Phys. Lett.* **1994**, *217*, 65–68.
- (5) Maurer, S. A.; Lambrecht, D. S.; Flaig, D.; Ochsenfeld, C. Distance-dependent Schwarz-based integral estimates for two-electron integrals: Reliable tightness vs. rigorous upper bounds. *J. Chem. Phys.* **2012**, *136*, 144107.
- (6) Thompson, T. H.; Ochsenfeld, C. Integral partition bounds for fast and effective screening of general one-, two-, and many-electron integrals. *J. Chem. Phys.* **2019**, *150*, 044101.
- (7) Dyczmons, V. No  $N^4$ -dependence in the calculation of large molecules. *Theor. Chim. Acta* **1973**, *28*, 307–310.
- (8) Häser, M.; Ahlrichs, R. Improvements on the direct SCF method. *J. Comput. Chem.* **1989**, *10*, 104–111.
- (9) Panas, I.; Almlöf, J.; Feyereisen, M. W. Ab initio methods for large systems. *Int. J. Quantum Chem.* **1991**, *40*, 797–807.
- (10) Baerends, E.; Ellis, D.; Ros, P. Self-consistent molecular Hartree—Fock—Slater calculations I. The computational procedure. *Chem. Phys.* **1973**, *2*, 41–51.

- (11) Whitten, J. L. Coulombic potential energy integrals and approximations. *J. Chem. Phys.* **1973**, *58*, 4496–4501.
- (12) Sambe, H.; Felton, R. H. A new computational approach to Slater’s SCF–X  $\alpha$  equation. *J. Chem. Phys.* **1975**, *62*, 1122–1126.
- (13) Dunlap, B. I.; Connolly, J. W. D.; Sabin, J. R. On some approximations in applications of X $\alpha$  theory. *J. Chem. Phys.* **1979**, *71*, 3396–3402.
- (14) Vahtras, O.; Almlöf, J.; Feyereisen, M. Integral approximations for LCAO-SCF calculations. *Chem. Phys. Lett.* **1993**, *213*, 514–518.
- (15) Eichkorn, K.; Weigend, F.; Treutler, O.; Ahlrichs, R. Auxiliary basis sets for main row atoms and transition metals and their use to approximate Coulomb potentials. *Theor. Chem. Acc.* **1997**, *97*, 119–124.
- (16) Weigend, F.; Köhn, A.; Hättig, C. Efficient use of the correlation consistent basis sets in resolution of the identity MP2 calculations. *J. Chem. Phys.* **2002**, *116*, 3175–3183.
- (17) Neese, F. An improvement of the resolution of the identity approximation for the formation of the Coulomb matrix. *J. Comput. Chem.* **2003**, *24*, 1740–1747.
- (18) Eichkorn, K.; Treutler, O.; Öhm, H.; Häser, M.; Ahlrichs, R. Auxiliary basis sets to approximate Coulomb potentials. *Chem. Phys. Lett.* **1995**, *240*, 283–290.
- (19) Weigend, F. Accurate Coulomb-fitting basis sets for H to Rn. *Phys. Chem. Chem. Phys.* **2006**, *8*, 1057–1065.
- (20) Weigend, F. A fully direct RI-HF algorithm: Implementation, optimised auxiliary basis sets, demonstration of accuracy and efficiency. *Phys. Chem. Chem. Phys.* **2002**, *4*, 4285–4291.
- (21) Eichkorn, K.; Treutler, O.; Öhm, H.; Häser, M.; Ahlrichs, R. Auxiliary basis sets to approximate Coulomb potentials. *Chem. Phys. Lett.* **1995**, *240*, 283–290.

- (22) Skylaris, C.-K.; Gagliardi, L.; Handy, N. C.; Ioannou, A. G.; Spencer, S.; Willetts, A. On the resolution of identity Coulomb energy approximation in density functional theory. *J. Mole. Struct.: THEOCHEM* **2000**, *501*, 229–239.
- (23) Van Faassen, M.; De Boeij, P.; Van Leeuwen, R.; Berger, J.; Snijders, J. Application of time-dependent current-density-functional theory to nonlocal exchange-correlation effects in polymers. *J. Chem. Phys.* **2003**, *118*, 1044–1053.
- (24) Gao, J.; Liu, W.; Song, B.; Liu, C. Time-dependent four-component relativistic density functional theory for excitation energies. *J. Chem. Phys.* **2004**, *121*, 6658–6666.
- (25) Beebe, N. H.; Linderberg, J. Simplifications in the generation and transformation of two-electron integrals in molecular calculations. *Int. J. Quantum Chem.* **1977**, *12*, 683–705.
- (26) Røeggen, I.; Wisløff-Nilssen, E. On the Beebe-Linderberg two-electron integral approximation. *Chem. Phys. Lett.* **1986**, *132*, 154–160.
- (27) Wilson, S. Universal basis sets and Cholesky decomposition of the two-electron integral matrix. *Comput. Phys. Commun.* **1990**, *58*, 71–81.
- (28) Koch, H.; Sánchez de Merás, A.; Pedersen, T. B. Reduced scaling in electronic structure calculations using Cholesky decompositions. *J. Chem. Phys.* **2003**, *118*, 9481–9484.
- (29) Pedersen, T. B.; Aquilante, F.; Lindh, R. Density fitting with auxiliary basis sets from Cholesky decompositions. *Theor. Chem. Acc.* **2009**, *124*, 1–10.
- (30) White, C. A.; Head-Gordon, M. Derivation and efficient implementation of the fast multipole method. *J. Chem. Phys.* **1994**, *101*, 6593–6605.
- (31) White, C. A.; Johnson, B. G.; Gill, P. M.; Head-Gordon, M. The continuous fast multipole method. *Chem. Phys. Lett.* **1994**, *230*, 8–16.

- (32) Kutteh, R.; Apra, E.; Nichols, J. A generalized fast multipole approach for Hartree-Fock and density functional computations. *Chem. Phys. Lett.* **1995**, *238*, 173–179.
- (33) Strain, M. C.; Scuseria, G. E.; Frisch, M. J. Achieving linear scaling for the electronic quantum Coulomb problem. *Science* **1996**, *271*, 51–53.
- (34) Challacombe, M.; Schwegler, E.; Almlöf, J. Fast assembly of the Coulomb matrix: A quantum chemical tree code. *J. Chem. Phys.* **1996**, *104*, 4685–4698.
- (35) Sierka, M.; Hogekamp, A.; Ahlrichs, R. Fast evaluation of the Coulomb potential for electron densities using multipole accelerated resolution of identity approximation. *J. Chem. Phys.* **2003**, *118*, 9136–9148.
- (36) Watson, M. A.; Salek, P.; Macak, P.; Helgaker, T. Linear-scaling formation of Kohn-Sham Hamiltonian: Application to the calculation of excitation energies and polarizabilities of large molecular systems. *J. Chem. Phys.* **2004**, *121*, 2915–2931.
- (37) Lazarski, R.; Burow, A. M.; Sierka, M. Density functional theory for molecular and periodic systems using density fitting and continuous fast multipole methods. *J. Chem. Theory Comput.* **2015**, *11*, 3029–3041.
- (38) Kohn, W. Density functional theory for systems of very many atoms. *Int. J. Quantum Chem.* **1995**, *56*, 229–232.
- (39) Schwegler, E.; Challacombe, M.; Head-Gordon, M. Linear scaling computation of the Fock matrix. II. Rigorous bounds on exchange integrals and incremental Fock build. *J. Chem. Phys.* **1997**, *106*, 9708–9717.
- (40) Schwegler, E.; Challacombe, M. Linear scaling computation of the Hartree-Fock exchange matrix. *J. Chem. Phys.* **1996**, *105*, 2726–2734.
- (41) Burant, J. C.; Scuseria, G. E.; Frisch, M. J. A linear scaling method for Hartree-Fock exchange calculations of large molecules. *J. Chem. Phys.* **1996**, *105*, 8969–8972.

- (42) Ochsenfeld, C.; White, C. A.; Head-Gordon, M. Linear and sublinear scaling formation of Hartree–Fock-type exchange matrices. *J. Chem. Phys.* **1998**, *109*, 1663–1669.
- (43) Schwegler, E.; Challacombe, M. Linear scaling computation of the Fock matrix. III. Formation of the exchange matrix with permutational symmetry. *Theor. Chem. Acc.* **2000**, *104*, 344–349.
- (44) Kussmann, J.; Ochsenfeld, C. Pre-selective screening for matrix elements in linear-scaling exact exchange calculations. *J. Chem. Phys.* **2013**, *138*, 134114.
- (45) Guidon, M.; Hutter, J.; VandeVondele, J. Auxiliary density matrix methods for Hartree–Fock exchange calculations. *J. Chem. Theory Comput.* **2010**, *6*, 2348–2364.
- (46) Früchtl, H. A.; Kendall, R. A.; Harrison, R. J.; Dyall, K. G. An implementation of RI–SCF on parallel computers. *Int. J. Quantum Chem.* **1997**, *64*, 63–69.
- (47) Weigend, F. Hartree–Fock exchange fitting basis sets for H to Rn. *J. Comput. Chem.* **2008**, *29*, 167–175.
- (48) Polly, R.; Werner\*, H.-J.; Manby, F. R.; Knowles, P. J. Fast Hartree–Fock theory using local density fitting approximations. *Mol. Phys.* **2004**, *102*, 2311–2321.
- (49) Sodt, A.; Head-Gordon, M. Hartree–Fock exchange computed using the atomic resolution of the identity approximation. *J. Chem. Phys.* **2008**, *128*, 104106.
- (50) Aquilante, F.; Lindh, R.; Bondo Pedersen, T. Unbiased auxiliary basis sets for accurate two-electron integral approximations. *J. Chem. Phys.* **2007**, *127*, 114107.
- (51) Reine, S.; Tellgren, E.; Krapp, A.; Kjærgaard, T.; Helgaker, T.; Jansik, B.; Høst, S.; Salek, P. Variational and robust density fitting of four-center two-electron integrals in local metrics. *J. Chem. Phys.* **2008**, *129*, 104101.

- (52) Aquilante, F.; Gagliardi, L.; Pedersen, T. B.; Lindh, R. Atomic Cholesky decompositions: A route to unbiased auxiliary basis sets for density fitting approximation with tunable accuracy and efficiency. *J. Chem. Phys.* **2009**, *130*, 154107.
- (53) Merlot, P.; Kjærgaard, T.; Helgaker, T.; Lindh, R.; Aquilante, F.; Reine, S.; Pedersen, T. B. Attractive electron–electron interactions within robust local fitting approximations. *J. Comput. Chem.* **2013**, *34*, 1486–1496.
- (54) Schwegler, E.; Challacombe, M.; Head-Gordon, M. A multipole acceptability criterion for electronic structure theory. *J. Chem. Phys.* **1998**, *109*, 8764–8769.
- (55) Schwegler, E.; Challacombe, M. Linear scaling computation of the Fock matrix. IV. Multipole accelerated formation of the exchange matrix. *J. Chem. Phys.* **1999**, *111*, 6223–6229.
- (56) Friesner, R. A. Solution of self-consistent field electronic structure equations by a pseudospectral method. *Chem. Phys. Lett.* **1985**, *116*, 39–43.
- (57) Neese, F.; Wennmohs, F.; Hansen, A.; Becker, U. Efficient, approximate and parallel Hartree–Fock and hybrid DFT calculations. A ‘chain-of-spheres’ algorithm for the Hartree–Fock exchange. *Chem. Phys.* **2009**, *356*, 98–109.
- (58) Izsák, R.; Neese, F. An overlap fitted chain of spheres exchange method. *J. Chem. Phys.* **2011**, *135*, 144105.
- (59) Helmich-Paris, B.; de Souza, B.; Neese, F.; Izsák, R. An improved chain of spheres for exchange algorithm. *J. Chem. Phys.* **2021**, *155*, 104109.
- (60) Maier, T. M.; Iwabata, Y.; Nakai, H. Efficient Semi-Numerical Implementation of Relativistic Exact Exchange within the Infinite-Order Two-Component Method Using a Modified Chain-of-Spheres Method. *J. Chem. Theory Comput.* **2019**, *15*, 4745–4763, PMID: 31403794.

- (61) Laqua, H.; Thompson, T. H.; Kussmann, J.; Ochsenfeld, C. Highly efficient, linear-scaling seminumerical exact-exchange method for graphic processing units. *J. Chem. Theory Comput.* **2020**, *16*, 1456–1468.
- (62) Laqua, H.; Kussmann, J.; Ochsenfeld, C. Accelerating seminumerical Fock-exchange calculations using mixed single-and double-precision arithmetic. *J. Chem. Phys.* **2021**, *154*, 214116.
- (63) Termath, V.; Handy, N. C. A Kohn-Sham method involving the direct determination of the Coulomb potential on a numerical grid. *Chem. Phys. Lett.* **1994**, *230*, 17–24.
- (64) van Wüllen, C. A hybrid method for the evaluation of the matrix elements of the Coulomb potential. *Chem. Phys. Lett.* **1995**, *245*, 648–652.
- (65) Delley, B. An all-electron numerical method for solving the local density functional for polyatomic molecules. *J. Chem. Phys.* **1990**, *92*, 508–517.
- (66) Liu, W.; Hong, G.; Dai, D.; Li, L.; Dolg, M. The Beijing four-component density functional program package (BDF) and its application to EuO, EuS, YbO and YbS. *Theor. Chem. Acc.* **1997**, *96*, 75–83.
- (67) Liu, W.; Wang, F.; Li, L. The Beijing density functional (BDF) program package: Methodologies and applications. *J. Theor. Comput. Chem.* **2003**, *2*, 257–272.
- (68) Rebolini, E.; Izsák, R.; Reine, S. S.; Helgaker, T.; Pedersen, T. B. Comparison of Three Efficient Approximate Exact-Exchange Algorithms: The Chain-of-Spheres Algorithm, Pair-Atomic Resolution-of-the-Identity Method, and Auxiliary Density Matrix Method. *J. Chem. Theory Comput.* **2016**, *12*, 3514–3522.
- (69) Laqua, H.; Thompson, T. H.; Kussmann, J.; Ochsenfeld, C. Highly efficient, linear-scaling seminumerical exact-exchange method for graphic processing units. *J. Chem. Theory Comput.* **2020**, *16*, 1456–1468.

- (70) Becke, A. D. A multicenter numerical integration scheme for polyatomic molecules. *J. Chem. Phys.* **1988**, *88*, 2547–2553.
- (71) Gill, P. M.; Johnson, B. G.; Pople, J. A. A standard grid for density functional calculations. *Chem. Phys. Lett.* **1993**, *209*, 506–512.
- (72) Lebedev, V. I. Values of the nodes and weights of ninth to seventeenth order gaussian quadrature formulae invariant under the octahedron group with inversion. *USSR Comput. Math. and Math. Phys.* **1975**, *15*, 44–51.
- (73) Lebedev, V. I. Quadratures on a sphere. *USSR Comput. Math. and Math. Phys.* **1976**, *16*, 10–24.
- (74) Krack, M.; Köster, A. M. An adaptive numerical integrator for molecular integrals. *J. Chem. Phys.* **1998**, *108*, 3226–3234.
- (75) Köster, A. M.; Flores-Moreno, R.; Reveles, J. U. Efficient and reliable numerical integration of exchange-correlation energies and potentials. *J. Chem. Phys.* **2004**, *121*, 681–690.
- (76) Valiev, M.; Bylaska, E. J.; Govind, N.; Kowalski, K.; Straatsma, T. P.; Van Dam, H. J. J.; Wang, D.; Nieplocha, J.; Aprà, E.; Windus, T. L.; others NWChem: A comprehensive and scalable open-source solution for large scale molecular simulations. *Comput. Phys. Commun.* **2010**, *181*, 1477–1489.
- (77) Liu, W.; Wang, F.; Lemin, L. In *Recent advances in relativistic molecular theory*; Hirao, K., Ishikawa, Y., Eds.; World Scientific: Singapore, 2004; pp 257–282.
- (78) Zhang, Y.; Suo, B.; Wang, Z.; Zhang, N.; Li, Z.; Lei, Y.; Zou, W.; Gao, J.; Peng, D.; Pu, Z.; Xiao, Y.; Sun, Q.; Wang, F.; Ma, Y.; Wang, X.; Guo, Y.; Liu, W. BDF: A relativistic electronic structure program package. *J. Chem. Phys.* **2020**, *152*, 064113.

- (79) Dunning Jr, T. H. Gaussian basis sets for use in correlated molecular calculations. I. The atoms boron through neon and hydrogen. *J. Chem. Phys.* **1989**, *90*, 1007–1023.
- (80) Zhao, Y.; Truhlar, D. G. Density Functional for Spectroscopy: No Long-Range Self-Interaction Error, Good Performance for Rydberg and Charge-Transfer States, and Better Performance on Average than B3LYP for Ground States. *J. Phys. Chem. A* **2006**, *110*, 13126–13130.
- (81) Zhao, Y.; Truhlar, D. G. The M06 suite of density functionals for main group thermochemistry, thermochemical kinetics, noncovalent interactions, excited states, and transition elements: two new functionals and systematic testing of four M06-class functionals and 12 other functionals. *Theor. Chem. Acc.* **2008**, *120*, 215–241.
- (82) Yanai, T.; Tew, D. P.; Handy, N. C. A new hybrid exchange–correlation functional using the Coulomb-attenuating method (CAM-B3LYP). *Chem. Phys. Lett.* **2004**, *393*, 51–57.
- (83) Grimme, S.; Antony, J.; Ehrlich, S.; Krieg, H. A consistent and accurate ab initio parametrization of density functional dispersion correction (DFT-D) for the 94 elements H-Pu. *J. Chem. Phys.* **2010**, *132*, 154104.
- (84) Adamo, C.; Scuseria, G. E.; Barone, V. Accurate excitation energies from time-dependent density functional theory: Assessing the PBE0 model. *J. Chem. Phys.* **1999**, *111*, 2889–2899.
- (85) Becke, A. D. Density-functional thermochemistry. III. The role of exact exchange. *J. Chem. Phys.* **1993**, *98*, 5648–5652.
- (86) Lee, C.; Yang, W.; Parr, R. G. Development of the colle-salvetti correlation-energy formula into a functional of the electron density. *Phy. Rev. B* **1988**, *37*, 785–789.

- (87) Staroverov, V. N.; Scuseria, G. E.; Tao, J.; Perdew, J. P. Comparative assessment of a new nonempirical density functional: Molecules and hydrogen-bonded complexes. *J. Chem. Phys.* **2003**, *119*, 12129–12137.
- (88) Perdew, J. P.; Burke, K.; Ernzerhof, M. Generalized gradient approximation made simple. *Phys. Rev. Lett.* **1996**, *77*, 3865.
- (89) Lehtola, S.; Steigemann, C.; Oliveira, M. J.; Marques, M. A. Recent developments in libxc — A comprehensive library of functionals for density functional theory. *SoftwareX* **2018**, *7*, 1–5.
- (90) Morgante, P.; Peverati, R. ACCDB: A collection of chemistry databases for broad computational purposes. *J. Comput. Chem.* **2019**, *40*, 839–848.
- (91) Huenerbein, R.; Schirmer, B.; Moellmann, J.; Grimme, S. Effects of London dispersion on the isomerization reactions of large organic molecules: a density functional benchmark study. *Phys. Chem. Chem. Phys.* **2010**, *12*, 6940–6948.
- (92) Goerigk, L.; Sharma, R. The INV24 test set: how well do quantum-chemical methods describe inversion and racemization barriers? *Can. J. Chem.* **2016**, *94*, 1133–1143.
- (93) Gao, J.; Zou, W.; Liu, W.; Xiao, Y.; Peng, D.; Song, B.; Liu, C. Time-dependent four-component relativistic density-functional theory for excitation energies. II. The exchange-correlation kernel. *J. Chem. Phys.* **2005**, *123*, 054102.
- (94) Peng, D.; Zou, W.; Liu, W. Time-dependent quasirelativistic density-functional theory based on the zeroth-order regular approximation. *J. Chem. Phys.* **2005**, *123*, 144101.